

Perceiving Extrinsic Contacts from Touch Improves Learning Insertion Policies

Carolina Higuera^{1,2}, Joseph Ortiz¹, Haozhi Qi^{1,3}, Luis Pineda¹, Byron Boots², and Mustafa Mukadam¹

¹FAIR, ²University of Washington, ³UC Berkeley

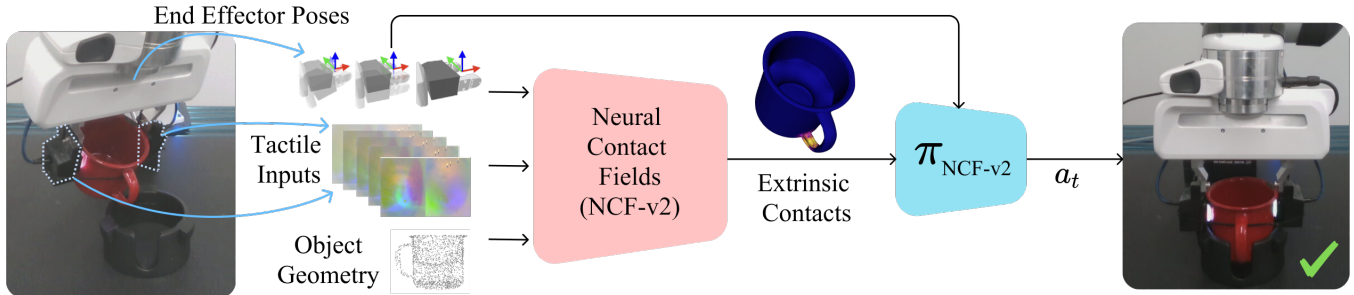


Fig. 1. Manipulation tasks such as inserting a mug in a cupholder involve interactions (extrinsic contacts) between the mug (object) and the cupholder (environment). Our model NCF-v2 enables sim-to-real transfer for estimating extrinsic contacts from tactile sensing between the robot fingers and the object. We use this representation to learn insertion policies that can be directly transferred to the real-world.

Abstract—Robotic manipulation tasks such as object insertion typically involve interactions between object and environment, namely extrinsic contacts. Prior work on Neural Contact Fields (NCF) use *intrinsic* tactile sensing between gripper and object to estimate *extrinsic* contacts in simulation. However, its effectiveness and utility in real-world tasks remains unknown. In this work, we improve NCF to enable sim-to-real transfer and use it to train policies for mug-in-cupholder and bowl-in-dishrack insertion tasks. We find our model NCF-v2, is capable of estimating extrinsic contacts in the real-world. Furthermore, our insertion policy with NCF-v2 outperforms policies without it, achieving 33% higher success and $1.36\times$ faster execution on mug-in-cupholder, and 13% higher success and $1.27\times$ faster execution on bowl-in-dishrack.

I. INTRODUCTION

Contact is inevitable; is estimation optional? During mundane activities like inserting a mug in a holder we often leverage our sense of touch to infer when and where the mug is in contact with the holder. We use this feedback, for example, when the mug’s handle is stuck on top of the holder to guide it towards a position that allows for correct insertion. In this work, we study how robot manipulation policies can benefit from increased spatial awareness through estimation of extrinsic contacts.

Extrinsic contacts characterize the interactions between an object being manipulated and the environment. Such interactions are prevalent in contact-rich manipulation tasks, like peg insertion [1], [2], [3], packing [4], and tool manipulation (spatulas and wrenches) [5], [6]. Since ego-centric vision can be typically occluded or insufficient to capture subtle changes, modeling object-environment interactions would be challenging without heavy environmental and object instrumentation. Alternatively, tactile sensing can be more suitable to infer these interactions, albeit indirectly through sensing between robot hand and object.

Prior work on Neural Contact Fields (NCF) [7] tackles the

problem of estimating extrinsic contact between object and environment from vision-based tactile sensors on the gripper holding the object. It trains a neural field to estimate the probability of any 3D point on the object surface being in extrinsic contact without making any assumptions about the geometry of the contact. NCF is able to localize multiple contact patches, captures contact/no-contact transitions, and generalizes to novel objects shapes in known categories. While these capabilities are a significant jump from related work at the time [8], [9], the results are limited to simulation and its applicability to downstream tasks is unexplored.

In this work, we analyze NCF [7] in the real world and observe that the tactile embeddings in the model are prone to real-world sensory noises and the recurrent structure of the contact regressor leads to error accumulation. We make simple yet significant improvements to the tactile embedding and contact regressor, such that our model NCF-v2 can transfer to the real-world. Then, we use this representation to train policies in simulation for mug-in-cupholder and bowl-in-dishrack insertion tasks, and directly transfer them to the real-world (Fig. 1). To analyze the impact of estimating extrinsic contacts on policy learning, we comprehensively evaluate four policies with different observation inputs: only using robot’s proprioception, with tactile data, with NCF-v2, and ground truth extrinsic contacts. We find that observability over extrinsic contacts leads to policies with consistently higher success rates and greater task efficiency measured through number of time steps to success.

II. RELATED WORK

Extensive work has explored localization and control of intrinsic contacts, i.e. interactions between end-effector and object, by focusing on internal forces of the grasp. Among those, it is common to use tactile sensing to obtain approximations of shear and normal forces of the grasp. Some works

explore maintaining sticking contact [10], [11] or use sliding dynamics [12], [13]. Recent work has also proposed an interesting and simple approach to fuse proximity and visuo-tactile point clouds for contact patch segmentation between the sensing membrane and objects [14].

Research on extrinsic contacts is an emerging topic in the robotics community. Extrinsic contacts are prominent in contact-rich manipulation tasks, for example, insertion, use of tools, and in general tasks that require controlling the interactions of a grasped object with the environment. Ma et al. [9] discuss a theoretical basis for localizing environmental contacts, solving a constraint optimization problem for three types of contact geometry: point, line, and patch. Kim et al. [15] propose a method to simultaneously estimate and control extrinsic contact with tactile feedback. A factor graph is used to fuse a sequence of tactile and kinematic measurements to estimate and control the interaction between gripper-object-environment.

For tool manipulation, Van der Merwe et al. [16] propose to learn a contact feature representation to predict the effects of the robot’s actions on the contact between the tool and the environment, based on visuo-tactile sensing. This contact representation provides information about the binary contact state, the line of contact between the tool and the environment, and a predicted end-effector wrench. Along similar lines, Oller et al. [17] show a side application of their method as a tracker of line contact between tool-environment, by querying points on the estimated object’s SDF within a specific distance. Previous work on tracking extrinsic contacts has predominantly relied on touch sensing, utilizing either a force-torque sensor at the robot’s wrist or vision-based tactile sensors. In contrast, Kim et al. [18] propose a novel approach centered on learning to localize extrinsic contacts based solely on a single RGB-D camera view of the robot’s workspace. The work most similar to ours is Neural Deforming Contact Field (NDCF) [19], where complex 3D contact patches are represented with neural fields. NDCF jointly models object deformations and contact patches via implicit representations, using a partial point cloud of the object and end-effector wrench information. This method allows tracking contacts on a deformable sponge in different environments.

III. SIM-TO-REAL NEURAL CONTACT FIELDS

Our work builds on Neural Contact Fields (NCF) [7] and improves it on several fronts to enable sim-to-real transfer. In this section, we first briefly discuss the original NCF (Section III-A) which we will call NCF-v1 for clarity. Then, we discuss the challenges and observations of transferring it to the real-world, and our subsequently improved model (Section III-B) that we call NCF-v2.

A. NCF preliminaries (NCF-v1)

Neural Contact Fields [7] estimate the extrinsic contacts between surface points of an object and the environment. Given a set of n query 3D points of the object, it outputs the probability of contact for each of them.

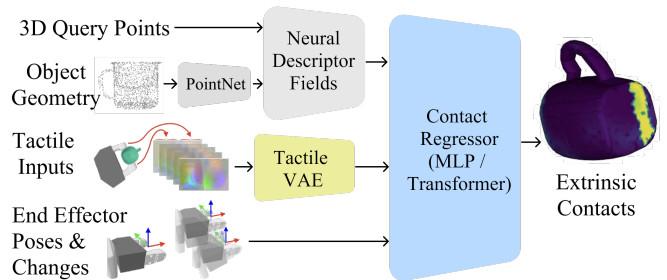


Fig. 2. Neural Contact Fields v2 (NCF-v2) architecture for tracking extrinsic contact (between object and environment) given tactile sensing (between robot hand and object). For a set of query 3D points on the object surface, NCF-v2 estimates the probability of any point in extrinsic contact.

NCF-v1 takes a shape representation, a history of end-effector poses, and a sequence of images from a vision-based touch sensor (e.g. DIGIT [20] is used in [7]) on the gripper as the inputs. Denoting $\mathbf{p}_t \in \mathbb{R}^n$ as the extrinsic contact probabilities where n is the number of query points, \mathbf{g}_t as the embedding of a sequence of tactile observations, \mathbf{r}_t as the object shape representation, \mathbf{e}_t as a sequence of end-effector poses. Then NCF-v1 is a function f with the following form:

$$\mathbf{p}_t = f_{\theta}(\mathbf{p}_{t-1}, \mathbf{g}_{t-1}, \mathbf{r}_{t-1}, \mathbf{e}_{t-1}). \quad (1)$$

It does not model the environment and only estimates local interactions between object and environments, and can generalize to unseen environments and shapes. However, the results in [7] are limited to simulation.

B. NCF improvements (NCF-v2)

In our experiments, we find it challenging to directly transfer NCF-v1 to the real-world. We observe two failure modes: 1) the tactile embedding \mathbf{g}_t is not accurate enough since real-world tactile information is more noisy; 2) the recurrent structure in the contact regressor leads to error accumulation. To address these problems, we make the following improvements. The final architecture for Neural Contact Fields is presented in Fig. 2.

Tactile Embedding. NCF-v1 trains an autoencoder to obtain tactile image embeddings at each timestep. A history of such embeddings is passed through a long short-term memory network (LSTM [21]) to derive the final representations \mathbf{g}_t for the sequence. We replace the autoencoder with a variational autoencoder [22] to learn a regularized embedding space and empirically find it beneficial for sim-to-real transfer. We also pre-process each image by subtracting the corresponding background image before encoding. This modification allows the network to prioritize reconstructing the contact rather than reconstructing background RGB values. To make the autoencoder robust to variations across different touch sensors, we also randomize over different background images. In total, we employed 24 background images from real DIGIT sensors. After we get the embedding for each tactile image, we concatenate T most recent embeddings and pass this vector through a Multi-layer Perceptron (MLP) instead of LSTM used in NCF. We choose $T = 5$ in our experiment and our sensor is sampled at 30 fps, which leads to ~ 0.17 seconds of tactile signal history.

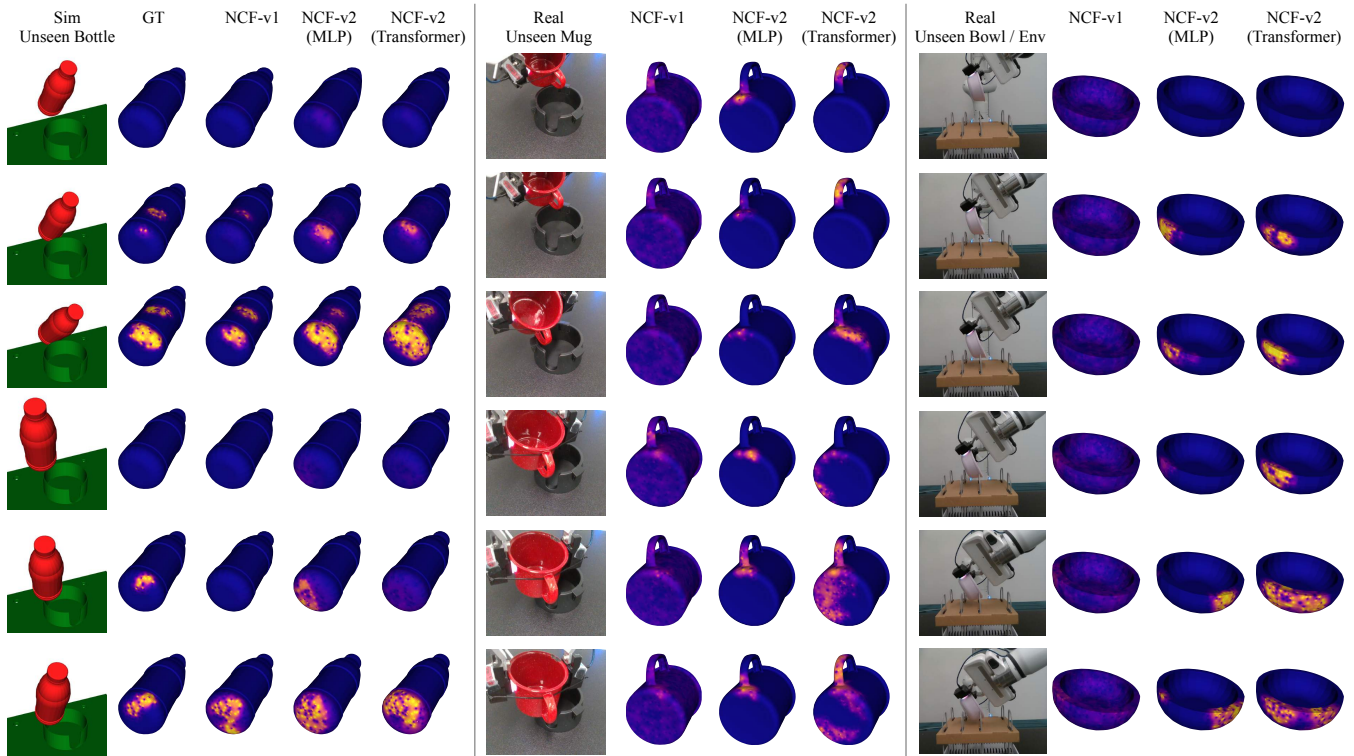


Fig. 3. **Qualitative study with unseen bottle (left), mug (middle), and bowl in unseen environment (right) in simulation (left) and real-world (middle and right).** The robot execute a predefined trajectory to make the object collide with the environment. We show estimated extrinsic contact patch from NCF-v1, NCF-v2 (MLP), and NCF-v2 (Transformer) on the object surface. In simulation, all models exhibit comparable performance in estimating extrinsic contact on unseen object shapes, accurately tracking contact/no-contact transitions, and localizing multiple contact patches. In the real world, NCF-v2 (Transformer) shows best sim-to-real performance in estimating extrinsic contacts.

Contact Regressor. NCF-v1 uses a recurrent structure to estimate the extrinsic contact probability. However, we find this design makes sim-to-real transfer particularly challenging, as the errors tend to accumulate over time, especially during long executions. Inspired by the recent advances in temporal sensory fusion methods [23], we remove this recurrent structure and only rely on the temporal cues from the inputs. Specifically, we remove p_{t-1} from Eq. (1), and directly concatenate the other inputs to form a feature vector for the current timestep. After that, we feed this vector to a temporal aggregation network to get the contact probability of each query point. We experiment with two types of temporal aggregation networks: MLP and transformer. The MLP version is a network with three layers, with output dimension [512, 128, 1]. Batch normalization and ReLU are appended after the first two hidden units. The transformer version is an encoder-only structure of two hidden layers with two heads. The feature dimension of transformer is 512 and the output is fed to two linear layers with output dimension [128, 1]. For both versions, a sigmoid activation in the end estimates the contact probability.

Training. We collect contact interactions using IsaacGym [24] and TACTO [25]. We simulate a Franka Panda arm equipped with a parallel gripper and DIGIT sensors on the gripper. The robot executes trajectories in a cupholder scene (Fig. 3, left) with three object categories collected from 3D Warehouse [26]: mugs, bottles, and bowls. We curated a dataset containing five different shapes for each category and

reserved one shape for testing shape generalization. All of the objects are initialized in a stable grasp pose. For neural descriptor field (NDF) [27], we follow the same setting as [7] and use a pretrained NDF to obtain a feature vector for each query point. We separately trained the DIGIT VAE using tactile images from the TACTO [25] simulator. See [7] for further details on prior architecture and training.

IV. NCF-v2 EVALUATION

We first quantitatively compare NCF-v1, NCF-v2 (MLP), NCF-v2 (Transformer) in simulation. We execute a predefined trajectory shown in Fig. 3 (left) to make the object collide with the environment (a cupholder in this experiment). All three models can successfully track contact/no-contact transitions and localize multiple contact patches with complex geometries and demonstrate similar performance in estimating the contact patch on the unseen bottle. We compute the Mean Squared Error (MSE) over 100 test trajectories involving unseen mugs, bottles, and bowls. The MSE for NCF-v1 is 0.048, NCF-v2 (MLP) is 0.042, and NCF-v2 (Transformer) is 0.039. The results for NCF-v1 are consistent with [7] in simulation.

However, when we deploy the trained models in the real-world, we observe the performance of NCF-v1 is significantly worse than NCF-v2. Fig. 3 (middle and right) shows the NCF-v2 (Transformer) model demonstrates superior performance in capturing the contacts occurring between object and environment. In the case of the unseen mug (middle), NCF-v2 (Transformer) effectively identifies the

contact points on the handle and smoothly transitions to detecting contact on the foot of the mug when it is positioned on the edge of the cupholder. NCF-v2 (MLP) captures the contact on the handle but struggles with tracking the transition. On the other hand, NCF-v1 fails to transfer to real-world data, mostly predicting zero contact everywhere. The predicted contact probabilities exhibit noise and the model faces difficulties in accurately localizing contacts.

We also evaluate generalization for unseen shape *and* environment (Fig. 3, right). NCF-v2 (MLP) and NCF-v2 (Transformer) effectively capture the transition from no-contact to contact. Both models capture the contacts as the bowl descends between the dividers, although NCF-v2 (Transformer) is more consistent, particularly towards the end of the trajectory when the bowl contacts the rack base while still situated between the dividers. As NCF-v2 (Transformer) consistently outperforms other variants in estimating extrinsic contacts on real data, we use it in the following experiments in learning policies for insertion tasks.

V. DOWNSTREAM TASKS USING NCF-v2

We explore the effectiveness of estimating extrinsic contacts in downstream tasks of mug-in-cupholder and bowl-in-dishrack, which involve contact-rich interactions between object and environment.

A. Experimental setup

Task 1: mug-in-cupholder. A Franka Panda arm with a parallel gripper and DIGIT sensors on each finger starts with a mug grasped above a table. The goal is to insert the mug in a cupholder on the table. The cupholder features a slot on the side, as depicted in Fig. 9 (top). Successful completion requires precise alignment ensuring the mug’s handle fits into the cupholder’s slot.

Task 2: bowl-in-dishrack. The robot starts with the bowl held above the dishrack. The goal is to insert the bowl into the second slot from the left, as depicted in Fig. 9 (bottom). Successful completion requires approaching the target slot while maintaining awareness of the dividers.

For both tasks, the action space of the robot consists of 6-DOF transformations relative to the current end-effector pose, with the rotation expressed as axis-angle. These actions are set as the target for the joint-space IK controller. We use IsaacGym for simulating the tasks, using the Factory environments [28] as reference, and use TACTO for simulating the touch sensors. For training, we run 256 environments in parallel, introducing randomization to the end-effector pose and running each episode for 250 steps.

Policy learning. To have a clear understanding of the utility of estimating extrinsic contacts for policy learning, we train and compare the performance of four policies with different observation space, as illustrated in Fig. 4.

- **Proprioception Only**, π_{prop} . This policy only receives end-effector pose information at time steps t , $t-1$, and $t-2$. We define these inputs as $e_{t-2:t} \in \mathbb{R}^{21}$.
- **w/ Tactile**, π_{tac} . We augment the proprioceptive observations by incorporating the embedding of the sequence

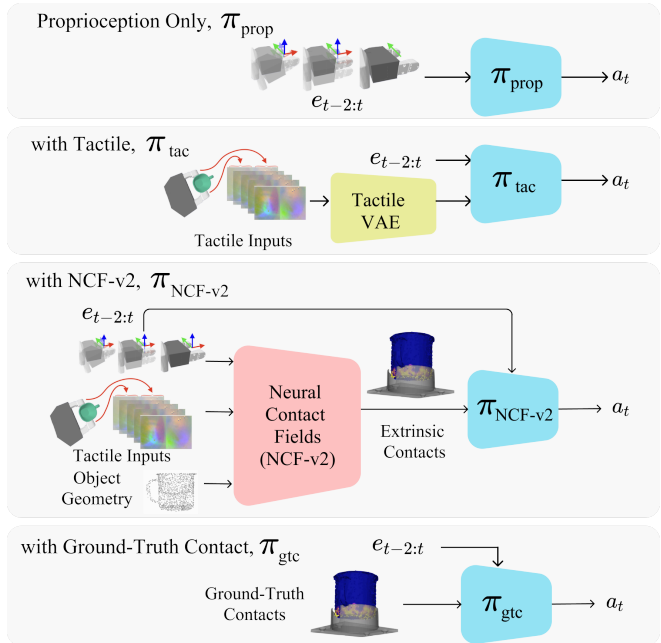


Fig. 4. **Overview of policies trained with different inputs.** We systematically study and compare the utility of estimating extrinsic contact in insertion tasks. We show explicitly estimate extrinsic contacts from tactile sensing is important for successful sim-to-real policies.

of tactile images. This is to test if directly incorporating tactile sensing is sufficient when compared to intermediate estimation of extrinsic contact.

- **w/ NCF-v2**, π_{NCF-v2} (ours): We augment the proprioceptive observations by including the estimated contact patch p_t using NCF-v2. This contact patch corresponds to the points on the object with a contact probability above a threshold. The contact patch is processed through an MLP and its feature embedding is extracted using max-pooling.
- **w/ Ground Truth Contact**, π_{gtc} (oracle): We augment the proprioceptive observations with the point cloud of the ground truth contact patch. It represents an upper bound for evaluation.

For each variant, we jointly optimize the policy π and the downsampling MLPs using PPO [29]. For the mug-in-cupholder, the reward function encourages the robot to approach the cupholder with the correct orientation, allowing the mug’s handle to fit into the cupholder’s slot: $r_t = -\lambda_{dist} r_{dist} - \lambda_{rot} r_{rot}$, where $r_{dist} = \|\mathbf{k}_m - \mathbf{k}_c\|_2$ penalizes the misalignment of four keypoints distributed along the mug central axis (\mathbf{k}_m) and the cupholder axis (\mathbf{k}_c). Additionally, $r_{rot} = \|\text{ref}_{rot} - \text{mug}_{rot}\|_2$ penalizes any deviation in the current orientation of the mug from a reference or goal orientation. For the bowl-in-dishrack task, the reward function seeks to minimize the misalignment between the position of the bowl p_{bowl} and target slot p_{target} : $r_t = -\|p_{bowl} - p_{target}\|_2$.

B. Task 1: mug-in-cupholder

Learning an insertion policy for this task is inherently challenging due to the narrow tolerance of 1 cm between the test

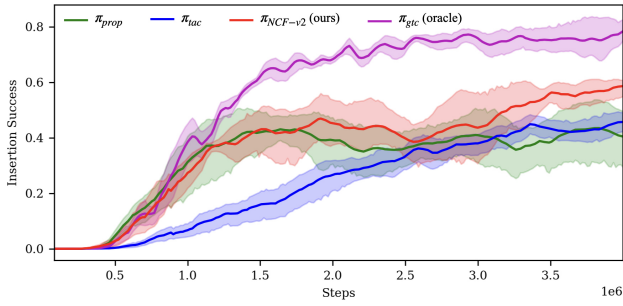


Fig. 5. Success rate mean and 95% confidence interval for mug-in-cupholder task across 256 parallel simulated environments. Each policy is trained with 5 seeds. π_{NCF-v2} (ours) outperforms policies using proprioception only or directly using tactile data.

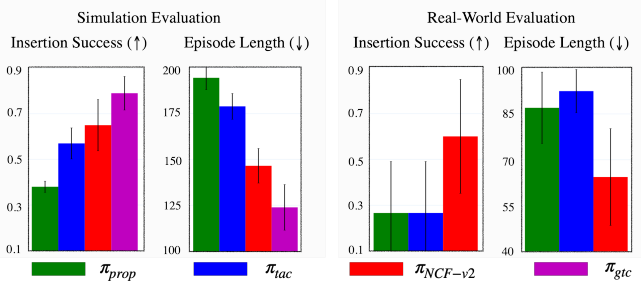


Fig. 6. **Evaluation of mug-in-cupholder policy.** We show insertion success and episode length of 100 trials in simulation (left) and 15 trials in real (right). π_{NCF-v2} (ours) performs better and faster compared to other policies that do not leverage extrinsic contact.

mug and the cupholder. While the robot can reduce keypoint misalignment, successful insertion ultimately hinges on the handle fitting into the slot. Fig. 5 illustrates the progression of the success rate during policy training. These learning curves strongly affirm the advantage of incorporating extrinsic contacts in learning policies for contact-rich tasks.

With access to ground truth extrinsic contacts, the policy achieves about 80% success rate in correctly inserting the mug. However, relying solely on the robot’s proprioception provides limited information, leading to early convergence to a low-performance policy. While π_{prop} is good at aligning the objects, it struggles with orienting the mug correctly. Integrating tactile information into the observations proves beneficial, but it demands extensive exploration to effectively map tactile signals to actions. π_{tac} requires nearly double the number of steps to achieve the same success rate as the proprioception-only policy. In contrast, a policy leveraging extrinsic contacts, like π_{NCF-v2} (ours) and π_{gtc} (oracle), demonstrates a relatively straightforward ability to align and orient the mug. This is facilitated by the availability of task-specific information, such as contacts on salient features of the object like the handle, body, and foot. π_{NCF-v2} (ours) exhibits a drop in performance but allows to localize extrinsic contacts in real-world.

We test all policies in simulation, running 100 repetitions. We also perform real-world experiments to evaluate π_{prop} , π_{tac} , and π_{NCF-v2} (ours) running 15 repetitions, without performing any fine-tuning. For each test, we randomize the initial end-effector pose. Fig. 6 presents the performance metrics for both simulation and real-world experiments. In

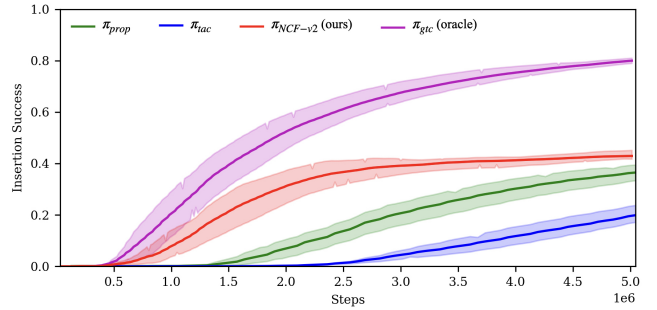


Fig. 7. Success rate mean and 95% confidence interval for bowl-in-dishrack task across 256 parallel simulated environments. Each policy is trained with 3 seeds. π_{NCF-v2} (ours) outperforms policies using proprioception only or directly using tactile data.

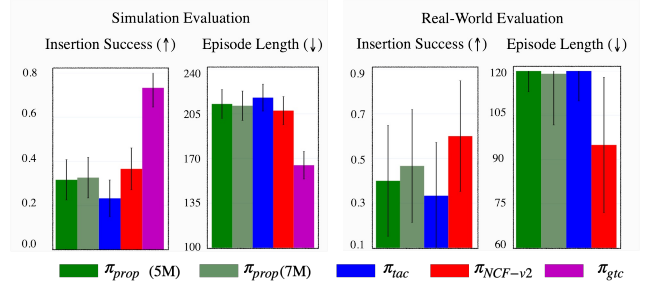


Fig. 8. **Evaluation of bowl-in-dishrack policy.** We show success and episode length of 100 trials in simulation (left) and 15 trials in real (right). π_{NCF-v2} (ours) performs better and faster compared to other policies that do not leverage extrinsic contact.

the simulation experiments, policies that incorporate extrinsic contact information demonstrate the highest success rates. Moreover, leveraging extrinsic contacts provides the additional benefit of learning policies capable of inserting the mug more efficiently in terms of the number of timesteps required to complete the task.

Ultimately, the real-world metrics are the strongest evidence of the utility of extrinsic contacts for the downstream task. π_{NCF-v2} (ours) has an average success rate of 60% over 15 repetitions, surpassing π_{prop} and π_{tac} at 27%. This represents an absolute improvement of 33%. Moreover, π_{NCF-v2} (ours) proves to be $1.36\times$ faster, finishing the task on average in 23 steps fewer than its counterparts, with each trial limited to a maximum of 100 steps.

C. Task 2: bowl-in-dishrack

This task requires spatial awareness in order to avoid collisions with the dividers when approaching the target slot and to leverage the dividers to guide the insertion. Fig. 7 shows the progression of the success rate during policy training. Having observability over extrinsic contacts proves to be very helpful for this task, especially when comparing the progression of the success rate for the oracle policy. Policies with only proprioceptive information or with raw tactile feedback require intensive exploration of the environment. Even with longer training π_{prop} cannot reach performance comparable to the oracle policy.

For training π_{NCF-v2} (ours), we are using the same model explained in Section III-B. This means that we are evaluating the ability of NCF-v2 to estimate useful extrinsic contacts for



Fig. 9. Successful policy executions on mug-in-cupholder (top) and bowl-in-dishrack (bottom) insertion tasks in real-world. On average, π_{NCF-v2} (ours) is 13 – 33% more successful and 1.27 – 1.36 \times faster at completing the tasks, compared to policies that do not leverage extrinsic contact.

a downstream task under both shape and environment generalization. However, given the small gap between the success rate seen after $5e6$ steps between π_{prop} and π_{NCF-v2} (ours), we train π_{prop} for $7e6$ steps to disambiguate the differences in performance when deploying the policies.

We test all policies in simulation, running 100 repetitions. We also perform real-world experiments to evaluate π_{prop} , π_{tac} , and π_{NCF-v2} (ours) running 15 repetitions, without performing any fine-tuning. For each test, we randomize the initial end-effector pose. Fig. 8 presents the performance metrics for both simulation and real-world experiments. In simulation, we find that with privileged contact information the policy correctly inserts the bowl in the desired slot in the dishrack around 75% of the time. However, the other policies exhibit a significantly lower performance. It is worth noting that in simulation we could not completely control the initial pose of the bowl due to undesired collisions with the gripper. Therefore, there was also a high degree of randomization in the initial bowl pose. While the oracle policy could implicitly provide information about the bowl’s pose through the contact point cloud, the other policies could not infer the bowl’s pose solely from the end-effector information. Even though NCF-v2 could estimate the contact pointcloud, it also relies on the end-effector to infer the object’s pose.

In the real-world experiments, the initial pose of the bowl is controlled, and all policies exhibit better performance. π_{NCF-v2} (ours) has the highest insertion rate, highlighting that NCF-v2 is generalizing to an unseen shape and environment. A policy with only proprioceptive information is not able to gather the spatial understanding that this task requires, even if trained for a longer time. π_{NCF-v2} (ours) achieves an absolute improvement of 13% in success rate with respect to π_{prop} and completes the bowl insertion 1.27 \times faster.

VI. CONCLUSION AND LIMITATIONS

In this work, we have demonstrated the utility of estimating extrinsic contacts from touch for learning robot insertion policies. Building upon prior work on NCF, we first made improvements to the tactile embedding and contact regressor to enable sim-to-real transfer of extrinsic contact estimation during real robot interactions. Through simulation and real-world evaluations, we verified our hypothesis that estimating extrinsic contact aids policy learning for two insertion tasks, mug-in-cupholder and bowl-in-dishrack. Policies with access to estimated/ground-truth extrinsic contacts achieve higher success rates than a baseline policy with access to only proprioception and to raw tactile data. In real-world experiments, policies with NCF-v2 outperform the baselines without fine-tuning, achieving 33% higher success and 1.36 \times faster execution on mug-in-cupholder, and 13% higher success and 1.27 \times faster execution on bowl-in-dishrack.

Limitations. The current NCF implementation is restricted to tracking extrinsic contacts for three specific object classes, assuming a fixed relative pose during grasping. Additionally, to get the correct reference point cloud, prior knowledge of the object class is necessary. To overcome these constraints, integrating NCF into a system that learns an implicit representation of various object shapes through vision can be advantageous.

ACKNOWLEDGMENT

The authors thank Tess Hellebrekers, Sudharshan Suresh, and Taosha Fan for helpful discussions, Raunaq Bhirangi for help with Franka controller, Mike Lambeta and Roberto Calandra for help with DIGIT sensor, and Elia Rühle for help with TACTO simulator.

REFERENCES

- [1] S. Dong, D. K. Jha, D. Romeres, S. Kim, D. Nikovski, and A. Rodriguez, "Tactile-rl for insertion: Generalization to objects of unknown geometry," in *International Conference on Robotics and Automation (ICRA)*, 2021.
- [2] G. Schoettler, A. Nair, J. Luo, S. Bahl, J. A. Ojea, E. Solowjow, and S. Levine, "Deep reinforcement learning for industrial insertion tasks with visual inputs and natural rewards," in *International Conference on Intelligent Robots and Systems (IROS)*, 2020.
- [3] L. Fu, H. Huang, L. Berscheid, H. Li, K. Goldberg, and S. inproceedingsChitta, "Safely learning visuo-tactile feedback policies in real for industrial insertion," in *International Conference on Robotics and Automation (ICRA)*, 2023.
- [4] S. Dong and A. Rodriguez, "Tactile-based insertion for dense box-packing," in *International Conference on Intelligent Robots and Systems (IROS)*, 2019.
- [5] Y. Wi, P. Florence, A. Zeng, and N. Fazeli, "Virdo: Visio-tactile implicit representations of deformable objects," in *International Conference on Robotics and Automation (ICRA)*, 2022.
- [6] A. Sipos and N. Fazeli, "Simultaneous contact location and object pose estimation using proprioception and tactile feedback," in *International Conference on Intelligent Robots and Systems (IROS)*, 2022.
- [7] C. Higuera, S. Dong, B. Boots, and M. Mukadam, "Neural contact fields: Tracking extrinsic contact with tactile sensing," in *International Conference on Robotics and Automation (ICRA)*, 2023.
- [8] S. Kim and A. Rodriguez, "Active extrinsic contact sensing: Application to general peg-in-hole insertion," in *International Conference on Robotics and Automation (ICRA)*, 2022.
- [9] D. Ma, S. Dong, and A. Rodriguez, "Extrinsic contact sensing with relative-motion tracking from distributed tactile measurements," in *International Conference on Robotics and Automation (ICRA)*, 2021.
- [10] F. Veiga, H. Van Hoof, J. Peters, and T. Hermans, "Stabilizing novel objects by learning to predict tactile slip," in *International Conference on Intelligent Robots and Systems (IROS)*, 2015.
- [11] M. Li, Y. Bekiroglu, D. Kragic, and A. Billard, "Learning of grasp adaptation through experience and tactile sensing," in *International Conference on Intelligent Robots and Systems (IROS)*, 2014.
- [12] S. Dong, D. Ma, E. Donlon, and A. Rodriguez, "Maintaining grasps within slipping bounds by monitoring incipient slip," in *International Conference on Robotics and Automation (ICRA)*, 2019.
- [13] Y. She, S. Wang, S. Dong, N. Sunil, A. Rodriguez, and E. Adelson, "Cable manipulation with a tactile-reactive gripper," *International Journal of Robotics Research (IJRR)*, 2021.
- [14] J. Yin, P. Shah, N. Kuppuswamy, A. Beaulieu, A. Uttamchandani, A. Castro, J. Pikul, and R. Tedrake, "Proximity and visuotactile point cloud fusion for contact patches in extreme deformation," *arXiv:2307.03839*, 2023.
- [15] S. Kim, D. K. Jha, D. Romeres, P. Patre, and A. Rodriguez, "Simultaneous tactile estimation and control of extrinsic contact," *arXiv:2303.03385*, 2023.
- [16] M. Van der Merwe, D. Berenson, and N. Fazeli, "Learning the dynamics of compliant tool-environment interaction for visuo-tactile contact servoing," in *Conference on Robot Learning (CoRL)*, 2023.
- [17] M. Oller, M. P. i Lisboa, D. Berenson, and N. Fazeli, "Manipulation via membranes: High-resolution and highly deformable tactile sensing and control," in *Conference on Robot Learning (CoRL)*, 2023.
- [18] L. Kim, Y. Li, M. Posa, and D. Jayaraman, "Vision-based contact localization without touch or force sensing," in *Conference on Robot Learning (CoRL)*, 2023.
- [19] M. Van der Merwe, Y. Wi, D. Berenson, and N. Fazeli, "Integrated object deformation and contact patch estimation from visuo-tactile feedback," *arXiv:2305.14470*, 2023.
- [20] M. Lambeta, P.-W. Chou, S. Tian, B. Yang, B. Maloon, V. R. Most, D. Stroud, R. Santos, A. Byagowi, G. Kammerer, *et al.*, "Digit: A novel design for a low-cost compact high-resolution tactile sensor with application to in-hand manipulation," *Robotics and Automation Letters (RA-L)*, 2020.
- [21] S. Hochreiter and J. Schmidhuber, "Long short-term memory," *Neural computation*, 1997.
- [22] D. P. Kingma and M. Welling, "Auto-encoding variational bayes," in *International Conference on Learning Representations (ICLR)*, 2014.
- [23] H. Qi, B. Yi, S. Suresh, M. Lambeta, Y. Ma, R. Calandra, and J. Malik, "General in-hand object rotation with vision and touch," in *Conference on Robot Learning (CoRL)*, 2023.
- [24] V. Makoviychuk, L. Wawrzyniak, Y. Guo, M. Lu, K. Storey, M. Macklin, D. Hoeller, N. Rudin, A. Allshire, A. Handa, and G. State, "Isaac gym: High performance gpu-based physics simulation for robot learning," in *NeurIPS Datasets and Benchmarks*, 2021.
- [25] S. Wang, M. Lambeta, P.-W. Chou, and R. Calandra, "Tacto: A fast, flexible, and open-source simulator for high-resolution vision-based tactile sensors," *Robotics and Automation Letters (RA-L)*, 2022.
- [26] "3d warehouse." [Online]. Available: <https://3dwarehouse.sketchup.com/?hl=en>
- [27] A. Simeonov, Y. Du, A. Tagliasacchi, J. B. Tenenbaum, A. Rodriguez, P. Agrawal, and V. Sitzmann, "Neural descriptor fields: Se (3)-equivariant object representations for manipulation," in *International Conference on Robotics and Automation (ICRA)*, 2022.
- [28] Y. Narang, K. Storey, I. Akinola, M. Macklin, P. Reist, L. Wawrzyniak, Y. Guo, A. Moravanszky, G. State, M. Lu, *et al.*, "Factory: Fast contact for robotic assembly," in *Robotics: Science and Systems (RSS)*, 2022.
- [29] J. Schulman, F. Wolski, P. Dhariwal, A. Radford, and O. Klimov, "Proximal policy optimization algorithms," *arXiv:1707.06347*, 2017.